The Journal of Chemical Physics ARTICLE scitation.org/journal/jcp

Non-isoplethic measurement on the solid–liquid–vapor equilibrium of binary mixtures at cryogenic temperatures

Cite as: J. Chem. Phys. 157, 064201 (2022); doi: 10.1063/5.0097465
Submitted: 28 April 2022 • Accepted: 27 June 2022 •
Published Online: 12 August 2022

Shaelyn M. Raposa,[1,a)] Sugata P. Tan,[2] William M. Grundy,[1,3] Gerrick E. Lindberg,[1] Jennifer Hanley,[1,3] Jordan K. Steckloff,[2,4] Stephen C. Tegler,[1] Anna E. Engle,[1] and Cecilia L. Thieberger[1]

AFFILIATIONS

[1] Department of Astronomy and Planetary Science, Northern Arizona University, Flagstaff, Arizona 86011, USA
[2] Planetary Science Institute, Tucson, Arizona 85719, USA
[3] Lowell Observatory, Flagstaff, Arizona 86001, USA
[4] University of Texas at Austin, Austin, Texas 78705, USA

Note: This paper is part of the JCP Special Topic on Fluids Meets Solids.
[a)] **Author to whom correspondence should be addressed:** smr676@nau.edu

ABSTRACT

We measured the solid–liquid–vapor (SLV) equilibrium of binary mixtures during experiments that alternated between cooling the mixture and injecting the more-volatile component into the sample chamber; thus, the composition of the mixture changed (non-isoplethic) throughout the experiment. Four binary mixtures were used in the experiments to represent mixtures with miscible solid phases (N_2/CO) and barely miscible solid solutions (N_2/C_2H_6), as well as mixtures with intermediate solid miscibility (N_2/CH_4 and CO/CH_4). We measured new SLV pressure data for the binary mixtures, except for N_2/CH_4, which are also available in the literature for verification in this work. While these mixtures are of great interest in planetary science and cryogenics, the resulting pressure data are also needed for modeling purposes. We found the results for N_2/CH_4 to be consistent with the literature. The resulting new SLV curve for CO/CH_4 shows similarities to N_2/CH_4. Both have two density inversion points (bracketing the temperature range where the solid floats). This result is important for places such as Pluto, Triton, and Titan, where these mixtures exist in vapor, liquid, and solid phases. Based on our experiments, the presence of a eutectic is unlikely for the N_2/CH_4 and CO/CH_4 systems. An azeotrope with or without a peritectic is likely, but further investigations are needed to confirm. The N_2/CO system does not have a density inversion point, as the ice always sinks in its liquid. For N_2/C_2H_6, new SLV pressure data were measured near each triple point of the pure components.

INTRODUCTION

Thermodynamic phase is a fundamental description of a material's behavior at a given state point (temperature, pressure, and composition); transitions between phases are central to understanding many phenomena. The phase behavior of a system is often represented with a phase diagram, which is a rich, detailed reservoir of thermodynamic information, with boundaries between phases denoted by phase curves. Because the evolution of physical systems can be mapped within such diagrams to understand how a system will evolve, significant effort has been invested in developing and applying methods to map phase behavior.

Phase diagrams and the information therein are used in many fields. Their utility in our everyday lives is often introduced with reference to water. The presence of water on Earth enables sunlight or internal heat to mobilize the material, translating thermal energy into the movement of the material that ultimately enables mechanical work to be performed on the environment. Familiar examples on the Earth include the evaporation of water from the sea surface and

its subsequent condensation and precipitation at higher altitudes, which feed rivers and glaciers that carve our landscape in spectacular ways. On Mars, the sublimation of seasonal polar deposits of carbon dioxide and water ice leads to diverse alien landforms. On the Saturnian moon Titan, mixtures of liquid methane, ethane, and nitrogen exhibit complex thermodynamic behavior that must be accounted for to understand the seasonal and limnological behaviors of Titan's polar lakes and seas (Malaska *et al.*, 2017; Hartwig *et al.*, 2018; and Steckloff *et al.*, 2020). Farther from the Sun, Pluto and the Neptunian moon Triton host a wide variety of terrains and landforms composed of, and formed through, the thermodynamic properties of nitrogen, carbon monoxide, and methane (e.g., Trafton *et al.*, 1998; McKinnon *et al.*, 2016; Trowbridge *et al.*, 2016; Moore *et al.*, 2017; Moores *et al.*, 2017; and Tegler *et al.*, 2019). Therefore, understanding the thermodynamic properties of these materials is crucial to understanding the thermodynamic evolution of their surfaces.

Nevertheless, there is a dearth of information for common volatile materials at the lower temperatures prevalent in the outer solar system, far from the Sun. There, many cosmically abundant volatile materials form solids held together with weak intermolecular forces that can be mobilized readily, despite the low temperatures and feeble energy inputs far from the Sun. Additionally, the prevalence of non-ideal molecular interactions within mixtures of chemical species leads to complexity beyond that seen in pure substances. However, the low temperatures required and diversity of possible mixtures present difficulty in studying these materials. Characterization of systems containing mixtures of small, weakly interacting molecules also has utility for numerous industrial applications. Three-phase solid–liquid–vapor (SLV) equilibrium is a valuable tool for optimizing and designing cryogenic processes in natural gas plants (Campestrini *et al.*, 2014). The solid–liquid equilibrium of cryogenic mixtures is also very important in designing refrigerants for cryocoolers (Robinson, 1995), where proper mixtures can be selected to reach sufficiently low temperatures without the formation of solids for clog-free operation (Maytal and Pfotenhauer, 2012). Therefore, it is useful to review how phase information is often gathered.

One approach is to examine phase behavior with molecular dynamics simulations. Molecular dynamic approaches calculate the forces acting on the atoms and molecules within a system to propagate molecular motion and interactions, from which the phase is seen to emerge from the dynamics at a given thermodynamic state point (Matsumoto *et al.*, 2002; Wales, 2012; Espinosa *et al.*, 2013; and Muniz *et al.*, 2021). Such an approach can and has been employed but can be complicated by ambiguous results. In fact, many approaches to deducing stable phase(s) can be frustrated by "traps," where unstable phases appear or persist despite being higher in free energy. Kinetic trapping in an out-of-equilibrium phase can occur when the timescale of the phase transition is longer than the timeframe of an experiment or when the state point changes too quickly for the system to respond and reach equilibrium. Relatedly, an unstable phase can persist if there is an energy barrier to forming the new phase or if the transition to the new phase requires large fluctuations to form a nucleation center.

Another approach is to alchemically explore the phase of a system, which can be done by biasing the system within the dynamics toward a phase or constructing a non-physical path that connects the phases to each other (Eike and Maginn, 2006; Kim and Straub, 2010; and Zhuang *et al.*, 2019). Such techniques are often time-consuming and only as faithful to experiment as the underlying molecular model used (Pinnick *et al.*, 2012). Thermodynamic models and equations of state can be developed to predict or reproduce phase behavior, but they rely on properties obtained from fundamental calculations or experiments. Inevitably, experimental preparation of a system and evaluation of the phase is required to characterize phase equilibrium.

The most common experiment used to measure the boundaries of solid–liquid phase equilibria (SLE) of binary mixtures is cooling at a constant composition (isopleth) of the mixture. The isoplethic cooling from the liquid phase detects the liquidus when the first chunk of the solid phase (ice) appears. The detection methods may vary from calorimetry, dilatometry, measurements of heat capacity, measurements of vapor pressure, visual detection of the solid phase, spectroscopy, diffraction, etc. (Moran, 1959; Omar *et al.*, 1962). Effective use of isopleths to determine a phase diagram requires accurate and precise determination of composition and dense sampling of compositions. Therefore, it is a demanding process to chart a whole liquidus curve with this technique. In this work, we present a straightforward alternative protocol that employs a combination of cooling and gas injection to map fluid–solid phase equilibria to trace liquidus/solidus curves in only a few experimental runs.

In this paper, we first describe the instrument and protocol to measure a liquidus curve with a few experiments. Next, we describe the modeling used to interpret and support the experimental results. Then, we report experimental results for four binary mixtures that have various solid-phase behaviors: from miscible (N_2/CO) to barely miscible (N_2/C_2H_6) and those in between (N_2/CH_4 and CO/CH_4). These binary mixtures have been selected primarily because of their importance for planetary studies in the outer solar system, but they are also of interest in cryogenics. Finally, we suggest prospects for the next steps for the proposed experimental method we introduce and offer conclusions drawn from our results.

EXPERIMENTAL SETUP AND METHOD

Instrument and materials

The experiments described in this paper were performed in an enclosed cryogenic cell in the Astrophysical Materials Laboratory at Northern Arizona University. The system has been described in several prior publications (e.g., Grundy *et al.*, 2011; Ahrens *et al.*, 2018; Tegler *et al.*, 2012; 2019; and Engle *et al.*, 2021), so only a brief description is provided here. The cell is composed of aluminum alloy, with a cylindrical sample volume 5 mm in length and 15 mm in diameter. Sapphire windows are forced against indium wire gaskets to cap both ends of the sample volume, permitting visual inspection and spectrometric measurements in both transmission and reflection geometry. The cell is cooled from below by a two-stage CTI 1050 closed-cycle helium refrigerator. A Cryo-Con model 24 C temperature controller monitors a pair of DT-670 silicon diode thermometers mounted immediately above and below the sample volume, with estimated measurement errors not larger than ±0.5 K. The temperature controller supplies power to a 50 **Ω** heater to hold

the cell at the desired temperature. Two such nichrome heaters are available: one wrapped above and one below the sample volume. Since the cell is cooled from below, a vertical thermal gradient exists across the sample volume, with the top of the cell being warmer than the bottom. If the top heater is used to control the temperature, the temperature difference between the top and bottom of the cell is a little over a Kelvin, whereas if the lower heater is used, the gradient is a few tenths of a Kelvin. The lower heater was used in the studies described in this paper. Materials to be studied are supplied from a series of high-pressure gas cylinders connected to a mixing manifold. Suppliers and reported purities of the gases used are listed in Table I.

Gases are mixed to the desired starting composition in a 2 L stainless steel mixing volume at room temperature before condensing them in the pre-cooled cell. Pressure is monitored at the mixing volume using an MKS Baratron model 627 F heated capacitance manometer sensitive to the range from 1 to 5000 Torr, with a reported precision of ±0.25% of the measured pressure. We performed tests using pure nitrogen, methane, and argon in equilibrium at their triple points, confirming the calibration of the pressure gauge. Small temperature offsets between DT-670 diode readings and the known phase change temperatures were corrected by means of a linear correction fitted to the measured triple point temperatures of N_2 and CH_4, plus a measurement of the temperature of the N_2 ice alpha-beta phase transition known to occur at 35.61 K (Scott, 1976). However, we observe slow zero-point drifts of as much as half a Torr over a day, so in this paper, we report pressure uncertainties of ±0.5 Torr. The stainless-steel fill tube between the cell and the mixing volume is about 2 m long, with an interior diameter of 4 mm, so gas moves in bulk along the fill tube, but there is little opportunity for diffusive separation. The last 30 cm of the fill tube is thin-walled stainless steel bellows tubing to provide mechanical flexibility during installation and maintenance and minimize conductive heat leakage into the cell along the fill tube.

Method

Using this laboratory setup, a combination of cooling and gas injection can be used to measure fluid–solid phase equilibria. For the binary mixtures in this work (N_2/CH_4, CO/CH_4, N_2/C_2H_6, N_2/CO), an alternative method to isoplethic cooling is applied to measure the liquidus, i.e., the phase boundary where the solid phase appears for the first time upon cooling. Because liquid and solid are practically incompressible phases at low pressures, the presence of vapor in the equilibrium does not effectively change the liquidus. The change is not detectable as it is well buried in the experimental error. Therefore, the presence of vapor as the pressurizing fluid in our experiments means that the measurements detect the three-phase SLV equilibrium on the liquidus. Experiments for these binary mixtures begin with the less-volatile component. For example, the N_2/CH_4 system experiments start with methane or a CH_4-rich mixture. For the next run of uncompleted experiments, the initial CH_4-rich sample can be premixed in the mixing volume at room temperature before injection into the cell. This mixing process occurs while the cell is cooling to the desired cryogenic starting temperature. The pressures of individual components can be used to approximate the compositions at which the previous run stopped. The ideal gas law is assumed such that the total pressure equals the sum of the partial pressures. For example, if the starting composition is 75% CH_4 and 25% N_2, 300 Torr of CH_4 and 100 Torr of N_2 would be added to the mixing volume. The method of measuring the three-phase SLV equilibria is similar to that used by Browning (1964), with a modification where the composition is also changed by injections of the more volatile pure component and, thus, can scan through all compositions. Browning applied injections of mixtures with known fixed compositions to change only the pressure between the liquidus and solidus of the mixtures.

The gas mixture is allowed to condense into the pre-cooled cell until it is just under half full of liquid; this allows room for more gas injection throughout the experiment. Because the initial equilibrium phases are vapor and liquid (i.e., in a vapor–liquid equilibrium—VLE), we determine the temperature and pressure of the liquidus when the first chunk of the solid phase is observed. We also call solid phases ices in this work. If the cooling continued, the system would eventually lose all the liquid by freezing into solid at the solidus, i.e., the condition at which the last drop of liquid exists before complete freezing. However, the detection of the last drop of liquid is not a trivial job (Moran, 1959), so we do not pursue this cooling path but push the system back into VLE by injecting more volatile gas (e.g., N_2 in N_2/CH_4 case) before further cooling to find the next liquidus point at a different composition. The injections give pressure to the system and, at the same time, change the total mixture composition in the system to become richer with the more volatile component. At each liquidus point, temperature and pressure are noted as well as qualitative properties of the ice, such as its density relative to the liquid (i.e., if it sinks or floats).

A significant advantage of this method is that the alternate cooling and injections can detect the three-phase equilibrium across the entire range of relevant temperatures without determining composition in advance. According to the phase rule, the three-phase SLV equilibrium pressure of binary mixtures is solely a function of temperature due to a single degree of freedom (univariant); this simplifies our measurements as the pressure will be fixed at a specified temperature as long as those three coexisting phases are present. Furthermore, if the binary mixtures have partially miscible solid phases at low temperatures, there may be an invariant condition where four phases (two solids, vapor, and liquid) can coexist in equilibrium; there are no degrees of freedom at this condition (invariant), so there is only one temperature and one pressure where this four-phase equilibrium occurs. The invariance is commonly known as the quadruple point, which can be a eutectic, a simple peritectic, or a peritectic with an azeotrope (Ricci, 1951). The eutectic is located at the minimum temperature of the three-phase

TABLE I. Suppliers and reported purities of the gases used in these experiments.

Gas	Supplier	Purity (%)
N_2	Praxair	99.999
CH_4	Airgas	99.999
CO	Airgas	99.99
C_2H_6	Airgas	99.99

SLV equilibrium, while the latter two are not. The simple peritectic has the minimum SLV temperature at the triple point of the more volatile component, while that with an azeotrope has the minimum at the azeotrope at a lower temperature. Therefore, if better equipped, the method also can determine the type of the quadruple point.

Another key advantage to this method is that density inversions (the condition when the ice changes from sinking to floating in its liquid, or vice versa) can be readily observed if the binary mixtures have them. Most pure substances sink in their liquids so that their mixtures also have solid phases that sink in their liquids, at least when the composition is rich with that pure component. However, some mixtures have their solids floating in their liquids at intermediate compositions. In this case, we have two density inversion points bracketing the temperature range where the solid floats.

Pure carbon monoxide (CO) is cooled from liquid to its solid phases to calibrate our experimental setup. CO is well known to have two distinct solid phases with different crystalline structures: the β-phase, which has a hexagonal closed packed (HCP) structure at higher temperatures, and the α-phase, which has a primitive/simple cubic (cP) structure at lower temperatures (Fukushima *et al.*, 1977). With the presence of vapor in our experiments, the system first settles into a VLE when the cooling starts. The β-solid-phase first appears at the SLV triple point, the data of which have been well documented in the literature. In this case, the thermodynamic degree of freedom is zero, so any starting temperature or pressure must lead to the invariant triple point upon cooling. The side product of this approach is that any equilibrium point along the cooling process represents the VLE above the triple point and vapor–solid equilibrium (VSE) below the triple point. In other words, the cooling process traces the vapor pressure of the condensed phases along the condensation and sublimation curves just in a single run of the experiment. Such a vapor-pressure measurement has also been demonstrated in isochoric condensation experiments using a calorimeter for VLE (Qiu *et al.*, 2018). As shown later in the results, further cooling will eventually reach the vapor–solid–solid (VSS) triple point, where the α-solid phase, β-solid phase, and vapor phase all coexist.

A significant drawback of this alternate cooling and injection method is that the liquidus composition must be measured using other means, e.g., using some optical device to measure them *in situ*, such as transmission or Raman spectroscopy. Nonetheless, the easiest way is to use an equation of state (EOS) to model the phase behavior that involves solid solutions of the mixtures. In this case, the experimental data of the SLV temperature and pressure can be used to derive the EOS parameter(s), and let the EOS calculate the liquidus compositions along with the solidus and other physical properties, such as the equilibrium phase densities. Such an EOS is available as described in the next section.

Modeling

Most EOS only deal with VLE, and only some can model equilibria with solid solutions, e.g., CRYOCHEM (Tan *et al.*, 2013) that applies the Perturbed-Chain Statistical Associating Fluid Theory (PC-SAFT) EOS (Gross and Sadowski, 2001) for the fluids and Lennard-Jones Weeks-Chandler-Andersen (LJ-WCA) model (Adidharma *et al.*, 2002; Adidharma and Radosz, 2004) for the solids, the LJ-SLV EOS (Campestrini *et al.*, 2014) that is based on the SLV cubic EOS (Yokozeki, 2003), and the solid solution approach applied with the translated Peng–Robinson cubic EOS for the fluids (Giraldo *et al.*, 2021). We use CRYOCHEM 2.0 EOS, an improved version of the original 2013 version that has proven reliable in representing solid-fluid equilibria at low to moderate pressures, such as that on Titan and Pluto (Tan and Kargel, 2018a; 2018b).

The three-phase equilibria of vapor V and condensed phases γ and σ are calculated based on the equilibrium requirements, i.e., the equality of the chemical potential (μ) of each individual component i in all the equilibrium phases,

$$\text{Pure compounds:}\quad \mu^{\mathrm{V}}(T,P) = \mu^{\gamma}(T,P) = \mu^{\sigma}(T,P), \tag{1}$$

$$\text{Binary mixtures:}\quad \mu_i^{\mathrm{V}}(\mathbf{x}^{\mathrm{V}},T,P) = \mu_i^{\gamma}(\mathbf{x}^{\gamma},T,P) = \mu_i^{\sigma}(\mathbf{x}^{\sigma},T,P),\quad i=1,2, \tag{2}$$

where T and P are the temperature and pressure, respectively, while $\mathbf{x}^{\mathrm{V}} = \{x_i\}^{\mathrm{V}}$ is the composition of the vapor phase in mole fractions; we use the notation γ and σ for the other condensed phases, which can be liquid or solid. For two-phase equilibria, Eqs. (1) and (2) can be used with only the first equation involving the chemical potentials in vapor V and the condensed phase γ, which may be liquid for VLE or solid for VSE.

The EOS, which is a Helmholtz free energy model, calculates the chemical potentials in Eqs. (1) and (2). As an example, the chemical potential of component i in phase V is calculated from the residual molar Helmholtz energy A^{R} through

$$\mu_i^{\mathrm{V}}(\mathbf{x}^{\mathrm{V}},T,P) = \Gamma_i(T) + RT\ln(x_i^{\mathrm{V}}P) + A^{\mathrm{R}} + \left(\frac{\partial A^{\mathrm{R}}}{\partial x_i^{\mathrm{V}}}\right)_{T,\rho^{\mathrm{V}},x_{j\neq i}^{\mathrm{V}}} - \sum_j x_j\left(\frac{\partial A^{\mathrm{R}}}{\partial x_j^{\mathrm{V}}}\right)_{T,\rho^{\mathrm{V}},x_{k\neq j}^{\mathrm{V}}} + \rho^{\mathrm{V}}\left(\frac{\partial A^{\mathrm{R}}}{\partial \rho^{\mathrm{V}}}\right)_{T,\mathbf{x}^{\mathrm{V}}} - RT\ln\left(1+\frac{\rho^{\mathrm{V}}}{RT}\left(\frac{\partial A^{\mathrm{R}}}{\partial \rho^{\mathrm{V}}}\right)_{T,\mathbf{x}^{\mathrm{V}}}\right), \tag{3}$$

where $\Gamma_i(T)$ is a function of temperature that is the same for all equilibrium phases and, thus, cancels out in the equalities of Eq. (2). In Eq. (3), the density ρ^{V} and the energy A^R belong to the phase V. R is the universal gas constant. The corresponding version for pure compound to be used in Eq. (1) can be derived directly from Eq. (3),

$$\mu^{V}(T,P) = \Gamma(T) + RT\ln(P) + A^{\mathrm{R}} + \rho^{\mathrm{V}}\left(\frac{\partial A^{\mathrm{R}}}{\partial \rho^{\mathrm{V}}}\right)_T - RT\ln\left(1+\frac{\rho^{\mathrm{V}}}{RT}\left(\frac{\partial A^{\mathrm{R}}}{\partial \rho^{\mathrm{V}}}\right)_T\right). \tag{4}$$

The expressions of chemical potentials for the other phases are in the same forms as Eqs. (3) and (4) with the correct phases. The expression in the last logarithm on the right-hand side of Eqs. (3) and (4) is used for calculating the system pressure. For mixtures,

$$\frac{P}{\rho^{\mathrm{V}}RT} = 1 + \frac{\rho^{\mathrm{V}}}{RT}\left(\frac{\partial A^{\mathrm{R}}}{\partial \rho^{\mathrm{V}}}\right)_{T,\mathbf{x}^{\mathrm{V}}}. \tag{5}$$

For pure compounds, the partial derivative in Eq. (5) is at constant T only. Note that in phase equilibria, the pressure is the same throughout all phases. Interested readers are referred to the original papers for the Helmholtz energy of the solid part (Tan and Kargel, 2018a; 2018b) and that of the fluid part of the EOS (Gross and Sadowski, 2001).

The EOS has two groups of parameters: one that describes the fluid and solid parameters for the pure components and another that describes the binary interaction parameters (BIP) for binary mixtures, which correct the interaction energy between unlike molecules through the mixing rule of the EOS. All pure-component parameters are derived from the experimental vapor pressure (VLE) and melting curve (SLE) of the compound. The fluid BIP is derived from the experimental VLE of the binary mixture, and solid BIP is derived from experimental liquidus (SLE) measurements. It is the latter BIP that is of interest for the EOS to validate, fine-tune, or even newly derive from the measurements in this work. All other parameters are taken from the literature (Tan and Kargel, 2018a; 2018b).

RESULTS AND DISCUSSION

In this section, we present the experimental data measured in our lab using the method described in the previous section and compare these results with the CRYOCHEM numerical model. All data are also tabulated in the supplementary material.

Pure gas: CO

Our cooling experiment started in the VLE region, as shown in the pressure–temperature (P–T) phase diagram in Fig. 1(a). The solid phase was observed to first appear at the triple point (triangle on the diagram). The triple point we observed, 68.1 K and 0.155 bar, agrees well with values reported in the literature, 68.1 K and 0.154 bar (Goodwin, 1985). Upon further cooling, all liquid froze, and then the system tracked down the VS equilibrium curve. The vapor pressures measured in the cooling process closely agree with previous work [see Fig. 1(a)]. The agreement of our results with previous work validates our instrument and measurements of the phase equilibria in the presence of the vapor phase.

Figure 1(b) shows straight lines according to the Clausius–Clapeyron (C–C) equation that divides the temperature range into three regions: VL at high temperatures, VS^{α} at low temperatures and VS^{β} at the intermediate temperature in between. These lines have slopes that represent the respective latent heat of phase transitions $\Delta H/R$,

$$\ln P^{\mathrm{VL}} = -\frac{\Delta H^{\mathrm{VL}}}{RT} + c_L, \tag{6}$$

$$\ln P^{\mathrm{VS}^{\alpha}} = -\frac{\Delta H^{\mathrm{VS}^{\alpha}}}{RT} + c_{\mathrm{S}^{\alpha}}, \tag{7}$$

$$\ln P^{\mathrm{VS}^{\beta}} = -\frac{\Delta H^{\mathrm{VS}^{\beta}}}{RT} + c_{\mathrm{S}^{\beta}}. \tag{8}$$

Pressures P's on the left-hand side are the vapor pressures of the respective condensed phases, while c's are the constants. The slope and constant of each line can be graphically correlated using linear regression. The resulting slopes, $\Delta H/R$, can then be used for estimating the latent heats, which are calculated to be 1554, 2222, and 1741 cal/mol, respectively. The literature data at the triple points are 1576, 1966, and 1775 cal/mol, respectively (Din, 1962). Therefore, the results are good enough considering that the C–C equation is

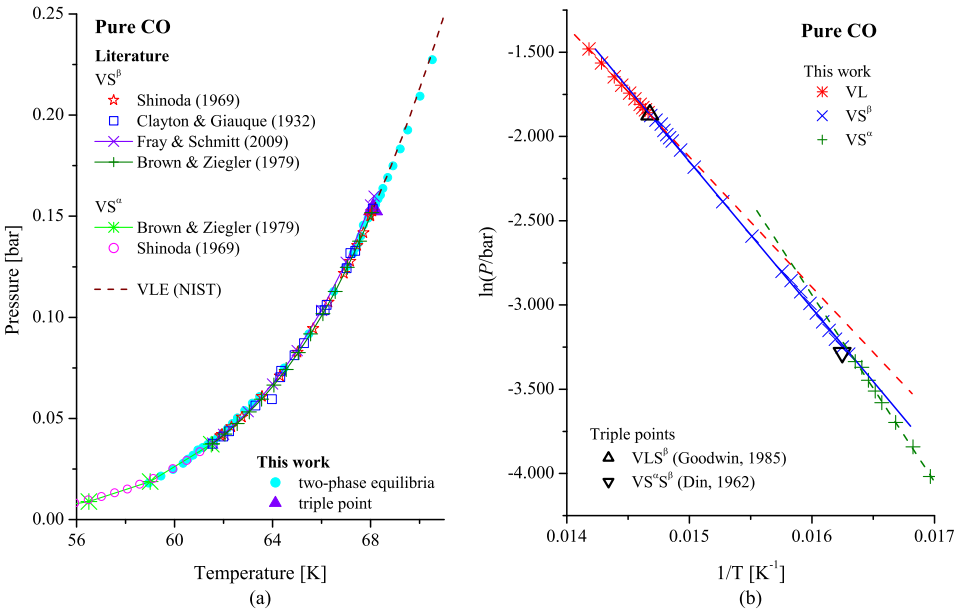

FIG. 1. Calibration of our experimental setup using pure carbon monoxide (CO) (cooled from liquid to its solid phases): (a) P–T phase diagram showing agreement between this work and the literature. (Shinoda, 1969;Clayton and Giauque, 1932; Fray and Schmitt, 2009; Brown and Ziegler, 1979). (b) Application of the Clausius–Clapeyron equation: solid and dashed lines are from linear regression for Eqs. (6)–(8).

derived by assuming ΔH to be constant with temperature, which is not true but approximately valid at low pressures.

The crossing points of these lines represent the three-phase equilibria, i.e., the triple points: VLS^{β} and $VS^{\alpha}S^{\beta}$ at high and low temperatures, respectively. However, the graphical method gives less accurate results, i.e., 67.6 K and 0.141 bar for VLS^{β} and 61.1 K and 0.035 bar for $VS^{\alpha}S^{\beta}$. The latter is 61.55 K and 0.037 bar in the literature (Din, 1962); unfortunately, it cannot be directly measured from visual observation with accuracy.

CRYOCHEM with the existing parameters for CO (Tan and Kargel, 2018b) describes the phase equilibria quite well, as shown in Fig. 2. The solid phase parameters were derived from the β-solid-liquid melting curve ($S^{\beta}L$), thus representing S^{β} in the EOS, while the parameters for S^{α} are not obtainable to our knowledge. Fortunately, the latter parameters are not needed for determining the liquidus of its binary mixtures in this work, the temperatures of which are all above the solid-solid-vapor triple point ($VS^{\alpha}S^{\beta}$). Nevertheless, as seen in Fig. 2, the calculated curve of VS^{β} may be extrapolated into the VS^{α} region without observable discrepancy, likely due to the small difference in the free energy of HCP and cubic crystalline structures (Adidharma and Tan, 2016). In future work, we will address this issue to better use the EOS in CRYOCHEM at conditions where the α-phase is the more stable of the two solid phases.

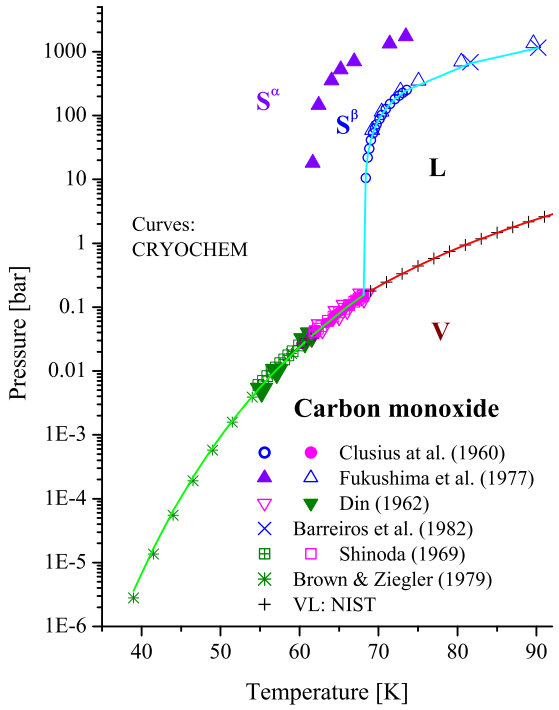

FIG. 2. The phase equilibria of pure CO as described by CRYOCHEM (curves). No calculation was made for the solid–solid boundary (filled triangles) due to the absence of parameters for solid S^{α}. Experimental data from the literature are shown as a comparison (Clusius *et al.*, 1960; Fukushima *et al.*, 1977; Fin, 1962; Barreiros *et al.*, 1982; Shinoda, 1969; Brown and Ziegler, 1979).

Binary N_2/CH_4: For verification of the current literature

The three-phase SLV data of this binary mixture are available in the literature (Omar *et al.*, 1962) but also verified using this method as this system is important to understand in the context of the solar system. On the Saturnian moon Titan, N_2 and CH_4 are present in the lakes and seas. Additionally, on Pluto and the Neptunian moon Triton, the landscapes are largely sculpted by N_2 and CH_4. Our measured data agree with Omar *et al.*, as shown in Fig. 3(a), which also shows the curve calculated using CRYOCHEM with the existing solid BIP (=0.57 derived by Tan and Kargel, 2018a; 2018b). Therefore, the BIP is confirmed to be valid, and the liquidus calculated using Eq. (2) is plotted together with the literature data in Fig. 3(b).

Because N_2 is more volatile than CH_4, it is used as the injected gas between the cooling processes. Therefore, the progression of the experiments started near pure CH_4 [1.0 CH_4 mole fraction; the right-hand side in Fig. 3(b)] and moved toward the N_2-rich region (0.0 CH_4 mole fraction) as N_2 was added. Each time we cool the mixture to the liquidus point at SLV equilibrium, where the solid first appears, further injection of N_2 sends the equilibrium back to VLE. The dotted arrows in Fig. 3(a) illustrate the alternate injection and cooling method. Horizontal arrows to higher pressures are the injections, while the slant arrows to lower temperatures are the cooling that inherently lowers the pressure.

For this binary mixture, we found that the upper density inversion near the maximum three-phase SLV pressure, i.e., when the solid phase, which sinks in its liquid at higher temperatures, becomes buoyant at lower temperatures, as observed in our previous experiment (Roe and Grundy, 2012; see also Hofgartner and Lunine, 2013). As seen in Fig. 4(a), liquid and solid densities become equal at the upper density inversion point. While the solid floats below the upper density inversion point in the lower part of the CH_4-rich branch on the phase diagram, it sinks in the N_2-rich branch such that there is a point at low temperature where a reverse density inversion occurs, the lower density inversion. For a mixture type with eutectic or peritectic, the lower density inversion is believed to occur at the eutectic/peritectic temperature where the four phases are in equilibrium: vapor, liquid, and two solids (CH_4-rich and N_2-rich solids in this case). At this temperature, the latter solid appears and eventually replaces the former when the cooling proceeds. The measured and calculated points of maximum pressure and density inversions are compared in Table II.

Figure 4(b) is the most commonly used phase diagram, also known as a condensed phase diagram for the SLV equilibrium (Ricci, 1951), where only the condensed phases are plotted. This means that the vapor is in the background. Every point on the phase boundaries is under its own vapor pressure, which is the three-phase SLV pressure.

Applying Eq. (2), in addition to the liquidus, CRYOCHEM also calculates the solidus, as shown in Fig. 4(b), which is significantly below the literature data points. In his dissertation, Moran (1959) acknowledged the difficulties in measuring the solidus of various binary mixtures due to the lack of homogeneity in the solid phase, thus resulting in large errors in his solidus data. Even though this may not be the sole reason for the deviation of the calculated solidus from the experimental data, the agreement of the predicted three-phase pressure data and the liquidus in Figs. 3(a)

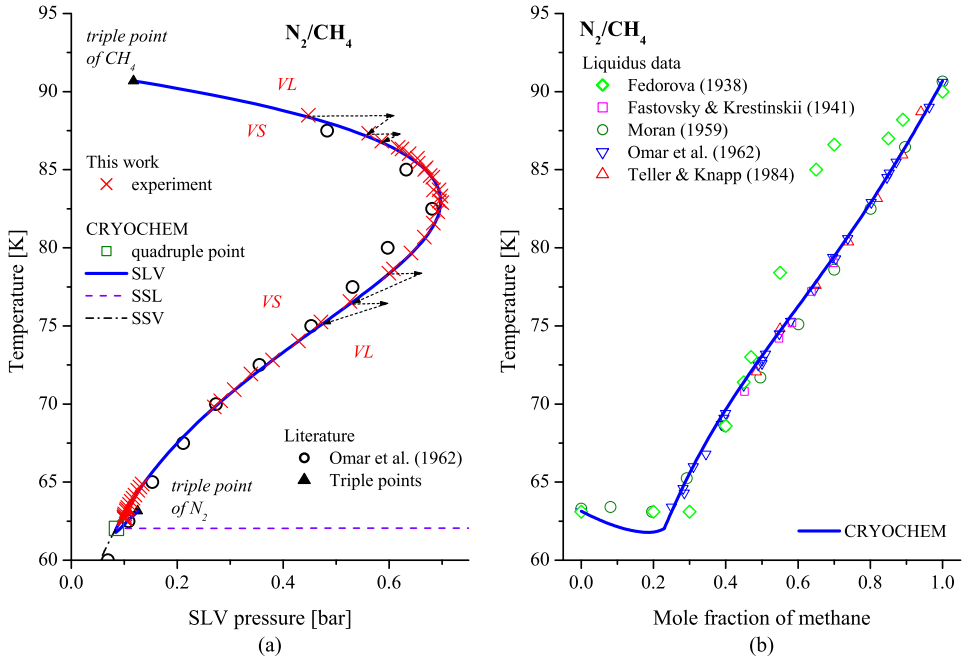

FIG. 3. Binary N_2/CH_4 compared to the literature: (a) Three-phase SLV *P–T* phase diagram; other three-phase curves are added for completeness. Dotted arrows are illustrations of the alternating injection (horizontal arrows) and cooling (slant arrows) used in this work; (b) Liquidus on the temperature–composition phase diagram. Curves are calculated using CRYOCHEM and compared to the literature (Fedorova, 1938; Fastovsky and Krestinskii, 1941; Moran, 1959; Omar *et al.*, 1962; Teller and Knapp, 1984).

and 3(b), as well as the upper density inversion in Table II, with the measurements, strongly implies self-consistency of the EOS. The disagreement in the lower SLV may then deserve to be investigated in the future because the consequences of such errors can be severe, such as the prediction of a peritectic followed by an azeotrope, as shown in Fig. 4(b), rather than a long-predicted eutectic (Omar *et al.*, 1962; Prokhvatilov and Yantsevich, 1983). Even though this conflict has not been disputed thus far for this binary mixture, it has for similar binary mixtures, i.e., nitrogen/argon, where experiments do not agree whether the mixture is of peritectic followed by azeotrope (Long and Di Paolo, 1963) or azeotropic type (Barret and Meyer, 1965), and argon/methane,

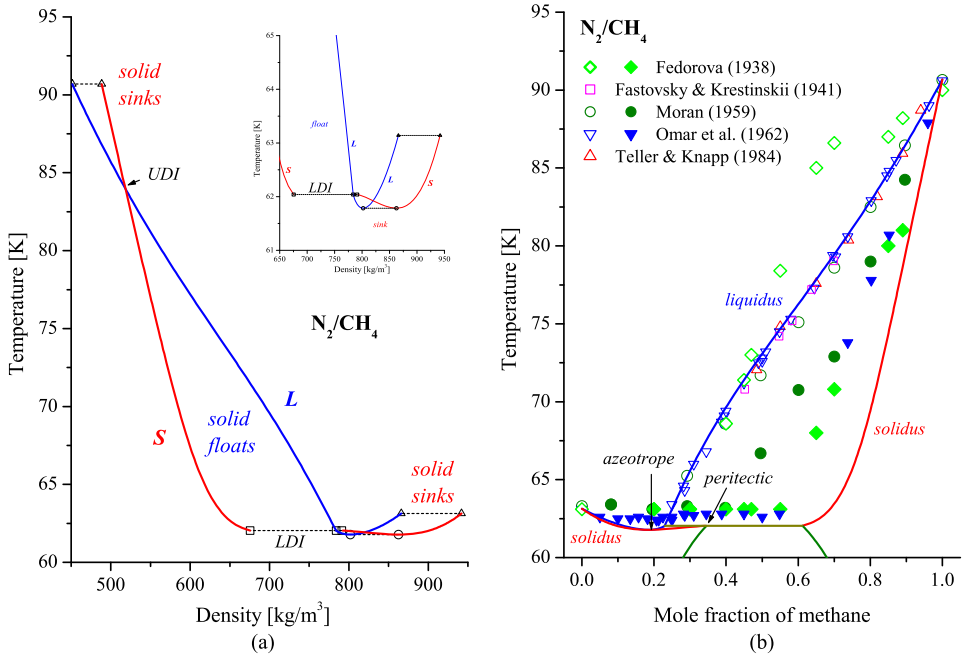

FIG. 4. Binary N_2/CH_4: (a) Density profiles of liquid and solid (UDI: upper density inversion, LDI: lower density inversion, solid floats between them), with the inset magnifying the region near the minimum SLV temperature; (b) Solidus, peritectic, and azeotrope on the condensed phase diagram; filled symbols: solidus data. All curves are calculated using CRYOCHEM 2.0.

TABLE II. Important points in the N_2/CH_4 mixture.

	Experiment		Literature		CRYOCHEM	
Point	T (K)	P (bars)	T (K)	P (bars)	T (K)	P (bars)
CH_4 triple point	⋯	⋯	90.68[a]	0.117	90.69	0.118
Upper density inversion	84.62	0.677	83.95[b]	⋯	83.97	0.690
Maximum pressure	82.89	0.699	⋯	⋯	82.97	0.697
Lower density inversion/eutectic/peritectic[c]	63.37	0.107	62.6[d]	0.110	62.04	0.085
Minimum temperature/azeotrope[c]	62.66	0.101	⋯	⋯	61.78	0.084
N_2 triple point	63.10	0.124	63.15[e]	0.125	63.14	0.126

[a] Younglove and Ely (1987).
[b] Roe and Grundy (2012)—mean value.
[c] This work cannot decisively determine the mixture type (eutectic or peritectic) but the lower density inversion and minimum temperature (the pressure is averaged from data at the same temperature).
[d] Omar *et al.* (1962).
[e] Span *et al.* (2000).

where experiments cannot decide whether it is a eutectic (Van 'T Zelfde *et al.*, 1968) or azeotropic type of mixture (Veith and Schroeder, 1937).

As described earlier, the eutectic temperature is the minimum temperature for the SLV, while it is not for the peritectic type with an azeotrope where the minimum temperature is instead at the azeotrope. As listed in Table II, our experiment found that the lower density inversion point, which is supposed to be at the eutectic/peritectic temperature, is not at the minimum temperature of the liquidus curve. This finding suggests that the binary N_2/CH_4 may not have the eutectic but instead an azeotrope. Nevertheless, our experiment could not confirm the presence of two coexisting solid phases at the lower density inversion point and, thus, cannot decisively determine the mixture type. If only a single solid phase is involved in the lower density inversion, then there is also a possibility for the mixture to be of an azeotropic type with completely miscible solid solution right below the azeotrope in the whole range of composition, but for this binary mixture, that would be in conflict with the results from x-ray diffraction study that shows unambiguously two immiscible coexisting solids in the temperature range of interest (Prokhvatilov and Yantsevich, 1983). These facts strongly suggest that this binary mixture has a peritectic followed by an azeotrope, but it is still an open issue to solve in future work.

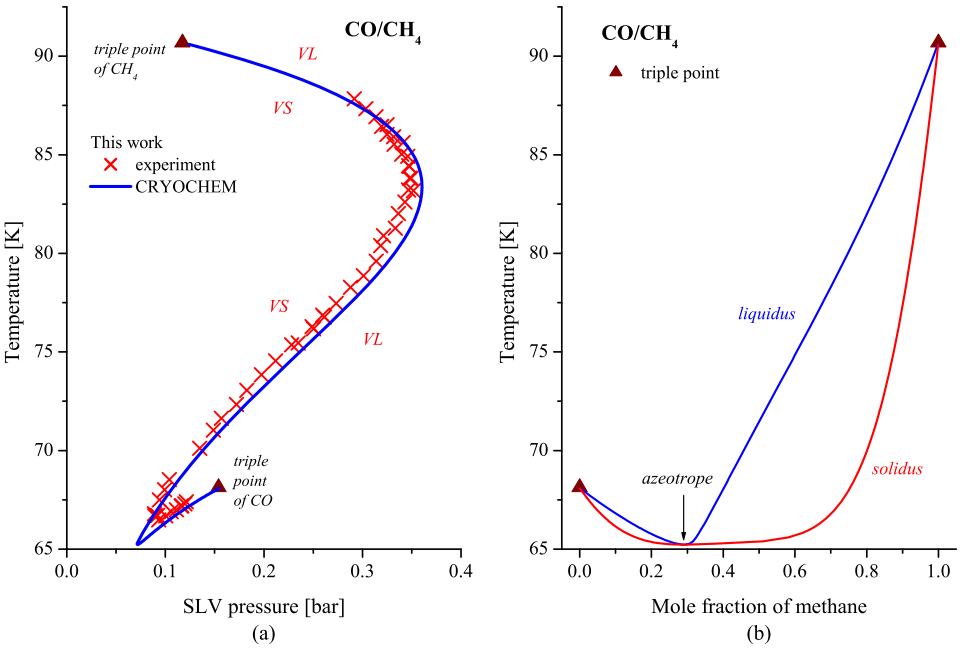

FIG. 5. New experimental data for binary CO/CH_4: (a) Three-phase SLV P–T phase diagram. (b) Liquidus and solidus on the temperature–composition condensed phase diagram. All curves: CRYOCHEM 2.0 with the new solid BIP (=0.075) derived according to SLV data in (a).

TABLE III. Important points in the CO/CH_4 mixture.

	Experiment (this work)		Literature		CRYOCHEM	
Point	T (K)	P (bars)	T (K)	P (bars)	T (K)	P (bars)
CH_4 triple point	···	···	90.68[a]	0.117	90.69	0.118
Upper density inversion	83.81–84.44	0.349–0.347	···	···	83.69	0.360
Maximum pressure	83.18	0.352	···	···	83.37	0.360
Lower density inversion	66.79–67.50	0.089–0.094	···	···	65.38	0.072
Azeotrope	66.68	0.100	···	···	65.23	0.072
CO triple point	68.10	0.153	68.13[b]	0.154	68.10	0.155

[a] Younglove and Ely (1987).
[b] Goodwin (1985).

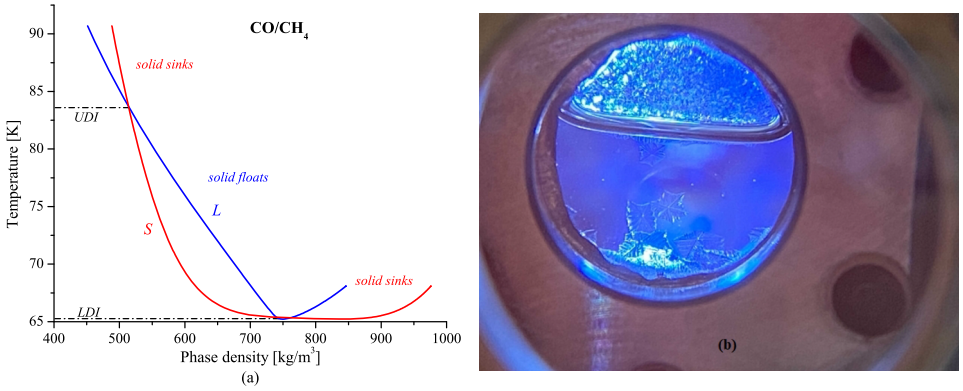

FIG. 6. Binary CO/CH_4: (a) density profiles of liquid and solid at SLV calculated using CRYOCHEM 2.0 (UDI: upper density inversion, LDI: lower density inversion, solid floats between them); (b) a snapshot of leaf-like CO-rich ice that sinks in its liquid (the blue coloration is caused by the anti-reflection coating on a lens associated with a spectrometer that was not used in this study).

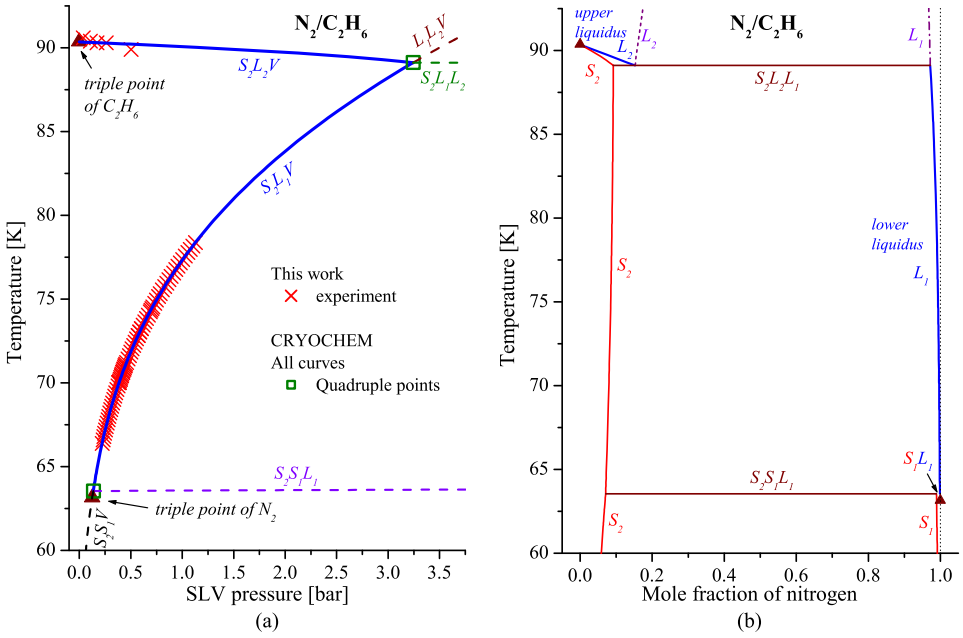

FIG. 7. Binary N_2/C_2H_6: (a) Three-phase SLV P–T phase diagram, other three-phase curves are added for completeness. (b) Liquidus (L_1 and L_2) and solidus (S_2) on temperature–composition condensed phase diagram. All curves: CRYOCHEM 2.0.

Binary CO/CH_4: New experimental data

In addition to N_2/CH_4, CO/CH_4 is also an important mixture at outer solar system planetary bodies, such as Pluto and Triton, where the ternary $N_2/CH_4/CO$ system dominates. The phase behavior of this binary mixture is expected to resemble that of N_2/CH_4 due to the close similarity of N_2 and CO. CO and N_2 are isoelectronic and have similar molecular weights, which result in similar thermodynamic properties such as their triple points, latent heats, and residence time behavior. Due to these similarities, they are often found together in deposits. Our experiments are the first ever to explore the low-temperature phase behavior of this mixture; no other experimental data is available in the literature. Based on the confidence obtained in experiments with binary N_2/CH_4 above, the measurements with alternate cooling and CO-injection did result in similar phase diagrams as shown in Fig. 5(a), which correspond to Fig. 3(a) for N_2/CH_4. The experimental SLV pressure and temperature are then used for deriving the solid BIP of CRYOCHEM, which is, in turn, used for calculating the liquidus and solidus in Fig. 5(b). The important points of this binary are listed in Table III.

Similar to that for N_2/CH_4, the lower density inversion point of CO/CH_4 is not at the minimum SLV temperature, which indicates the presence of an azeotrope with or without a peritectic. Again, as the experiment could not confirm the number of solid phases involved in the lower density inversion, the presence of peritectic cannot be decisively determined. This is subject to a future investigation, especially when the composition can be measured *in situ* to compare with the prediction of liquidus in Fig. 5(b). Therefore, at least for now, before it is experimentally proven otherwise, the current prediction by CRYOCHEM is followed, i.e., an azeotrope without a peritectic. This means that the solid miscibility gap, which is supposed to exist between two solids of different crystalline structures, such as in this binary (face-centered cubic for CH_4), does not touch the solid–liquid coexistence regions on the condensed phase diagram. The phase behavior on the CO-rich branch beyond the azeotrope was measured using the combination of CO-injection and heating instead of cooling by direct visual observation of vanishing solid that completely melts with heating.

The old solid BIP used in CRYOCHEM that was assumed to be the same as that of N_2/CH_4 due to the absence of experimental data (=0.057 in Tan and Kargel, 2018a; 2018b) is found to be inaccurate. The new solid BIP (=0.075) is then derived from the newly acquired data and used to construct the liquidus and solidus curves, as shown in Fig. 5(b). The predicted maximum pressure and the temperatures where the density inversions occur match the observation. The density inversion is illustrated in Fig. 6(a) at the upper density inversion at a higher temperature and the lower density inversion near the azeotrope. A snapshot of the CO-rich ice that sinks in its liquid is shown in Fig. 6(b).

TABLE IV. Important points in the N_2/C_2H_6 mixture.

	Literature		CRYOCHEM	
Point	T (K)	P (bars)	T (K)	P (bars)
C_2H_6 triple point	90.37[a]	1.14×10^{-5}	90.35	1.15×10^{-5}
Upper quadruple point	···	···	89.12	3.244
Lower quadruple point	···	···	63.55	0.136
N_2 triple point	63.15[b]	0.125	63.14	0.126

[a] Bücker and Wagner (2006).
[b] Span *et al.* (2000).

Binary N_2/C_2H_6: Barely miscible solid solutions

In addition to N_2/CH_4, N_2/C_2H_6 is important at Titan, where the ternary $N_2/CH_4/C_2H_6$ system dominates the lakes and seas. This binary mixture has barely miscible solutions not only for its liquid–liquid equilibrium as described in the literature (Llave *et al.*, 1985) but also for its solid–solid equilibrium as implied from large solid–liquid coexistence regions in experiments at high pressures (Wisotzki and Schneider, 1985). Based on the few latter data, the solid BIP of CRYOCHEM was derived and extrapolated for use at much lower pressures for applications on Titan (Tan and Kargel, 2018a). Therefore, the experiments in this work provide us with new data at low temperatures and low pressures to explore the phase behavior under these conditions.

As shown in Fig. 7(a), two data groups were measured, i.e., one at higher temperatures near the triple point of C_2H_6 and the other at lower temperatures near the triple point of N_2. Unfortunately, the experimental setup in this work cannot reach pressures much higher than atmospheric pressure, so the two

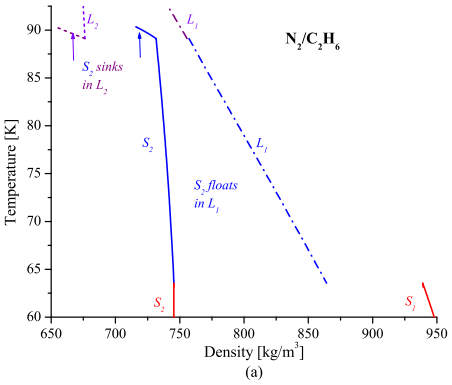

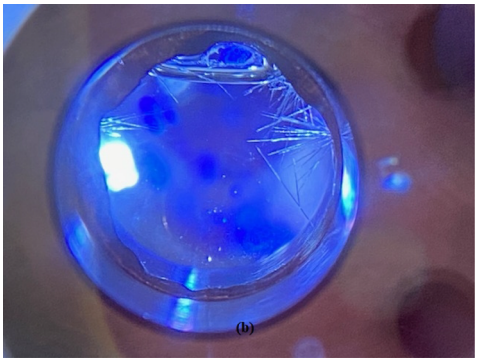

FIG. 8. Binary N_2/C_2H_6: (a) density profiles of liquid and solid at SLV calculated using CRYOCHEM 2.0; (b) a snapshot of needle-like C_2H_6-rich ice that floats in N_2-rich liquid L_1.

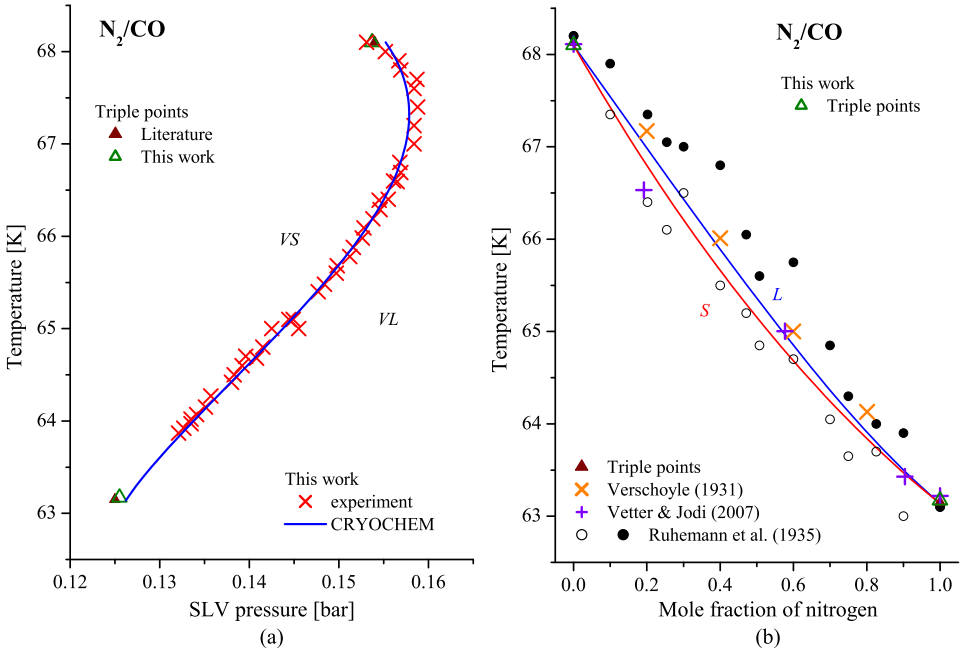

FIG. 9. Binary N_2/CO: (a) Three-phase SLV *P–T* phase diagram. (b) Liquidus and solidus on temperature–composition condensed phase diagram. All curves: CRYOCHEM 2.0 with a new solid BIP (=0.0162) derived from SLV data in (a). Triple points are from Goodwin (1985) and Span *et al.* (2000) and data is compared to Verschoyle(1931), Vetter *et al.*(2007) and Ruhemann *et al.*(1935).

groups of data cannot meet at the upper quadruple point where four phases (vapor, two liquids, and a solid phase—VLLS) are in equilibrium.

Using the existing solid BIP (=0.025 derived in Tan and Kargel, 2018a), CRYOCHEM can correctly predict the SLV curves, as shown in Fig. 7(a). The upper curve has a C_2H_6-rich liquid L_2, while the lower curve has an N_2-rich liquid L_1. The solid phase involved is C_2H_6-rich solid S_2 for both curves. The corresponding calculated liquidus and solidus diagram is shown in Fig. 7(b). Note that the upper quadruple point solid-liquid-liquid-vapor (SLLV) (monotectic on the condensed phase diagram) is calculated at about 90.35 K [practically at the solid-liquid-liquid (SLL) line], while the lower quadruple point solid-solid-liquid-vapor (SSLV) (simple peritectic on the condensed phase diagram) is at about 63.55 K [practically at the solid-solid-liquid (SSL) line, where the second solid is the N_2-rich solid S_1]. The upper liquidus curve is at the small branch near the C_2H_6 triple point, while the lower liquidus curve is between the upper and lower quadruple points [or the SLL and SSL lines on the condensed phase diagram Fig. 7(b)]. As calculated using CRYOCHEM, N_2 and C_2H_6 are almost entirely immiscible with huge phase-coexistence regions across the entire range of temperatures considered on the diagram in Fig. 7(b) at all possible phase equilibria. With an almost vertical profile of the lower liquidus on the diagram, the conventional isoplethic cooling method will be quite challenging to apply, while the three-phase SLV pressures are still obtainable through the alternate cooling and N_2-injection in this work. The important points for this binary mixture are listed in Table IV.

The calculated equilibrium phase densities shown in Fig. 8(a) are consistent with the experimental observations. Along the upper liquidus, the C_2H_6-rich solid sinks in its liquid L_2. On the other hand, it floats in N_2-rich liquid L_1 along the lower liquidus, as seen in Fig. 8(b).

Binary N_2/CO: Miscible solid phases

To reiterate, the ternary $N_2/CH_4/CO$ system dominates Pluto and Triton, shaping the geology and sculpting the unique

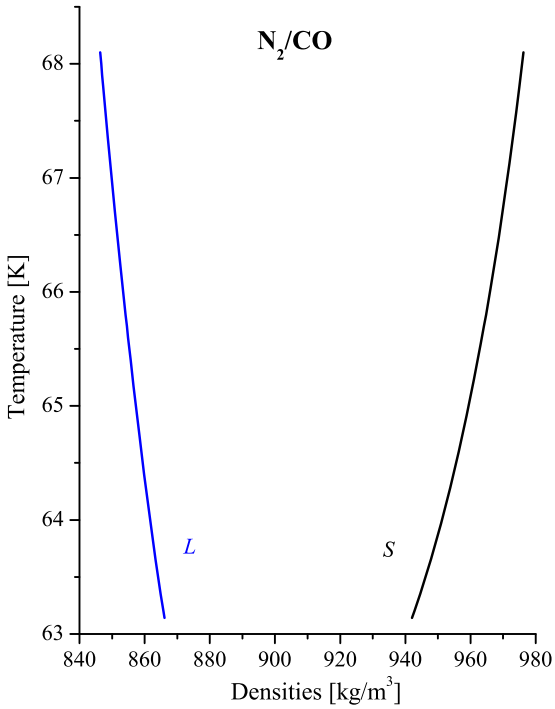

FIG. 10. Binary N_2/CO: density profiles of liquid and solid at SLV calculated using CRYOCHEM 2.0.

TABLE V. Important points in the N_2/CO mixture.

	Experiment (this work)		Literature		CRYOCHEM	
Point	T (K)	P (bars)	T (K)	P (bars)	T (K)	P (bars)
CO triple point	68.10	0.153	68.13[a]	0.154	68.10	0.155
Maximum pressure	67.40	0.159	···	···	67.32	0.158
N_2 triple point	63.17	0.126	63.15[b]	0.125	63.14	0.126

[a] Goodwin (1985).
[b] Span *et al.* (2000).

landscapes, making it necessary to understand the constituting binaries. Opposite to the binary N_2/C_2H_6, the binary N_2/CO has miscible solid phases at all compositions. Counter-intuitively, the similarity of the components results in inaccuracies in the measurements of the mixture. This is also evident from prior studies, which report results scattered around the narrow liquid–solid coexistence region shown in Fig. 9(b). The pressure and temperature ranges of the three-phase SLV equilibrium are narrower for this binary, so smaller gas injections and slower cooling rates were implemented so that many data points could still be collected along the SLV curve.

Figure 9(a) shows the measured three-phase SLV pressures and the corresponding CRYOCHEM correlation using its newly derived solid BIP (=0.0162), which is slightly different from the old one (=0.015 in Tan and Kargel, 2018b). The liquidus and solidus data available in the literature and the predicted curves by CRYOCHEM are shown together in Fig. 9(b).

While this binary mixture exhibits the maximum pressure as that in N_2/CH_4 and CO/CH_4, it has no density inversion. The density calculation and observation agree that the solid always sinks in its liquid, as also shown in Fig. 10, where the density of the solid is always larger than the liquid. The important points of this mixture are listed in Table V.

CONCLUSION

Employing this laboratory method of alternate cooling and gas injection, the three-phase SLV curves were successfully measured for the following binary systems: N_2/CO, N_2/C_2H_6, N_2/CH_4, and CO/CH_4. This selection of binary systems covers the range of mixtures with miscible solid phases (N_2/CO) to barely miscible (N_2/C_2H_6), with two in between (N_2/CH_4 and CO/CH_4). Studies of these systems are crucial for planetary science applications. N_2/CH_4/CO is an important ternary system for the evolution of planetary surfaces, such as on Pluto and Triton. Additionally, $N_2/CH_4/C_2H_6$ makes up the bulk composition of Titan's lakes and seas.

An advantage of this laboratory approach is that it enables us to measure many data points along the three-phase SLV curve in only a few experiments, as opposed to one data point in each run of conventional isoplethic experiments because this current method does not require the composition of the mixture to be determined in advance. Additionally, it can detect the density inversion if the mixture has one. The measured SLV pressure data are very useful for the development and improvement of models such as CRYOCHEM, which proves to be helpful in this work. The model can calculate the liquidus and solidus as well as the equilibrium phase densities. Its predictions on the density inversion points that match the observation serve as the validation of the model, even in the absence of the liquidus experimental data.

Our experimental results determined that the N_2/CH_4 three-phase SLV pressure data agrees with the data in the literature (Omar *et al.*, 1962), thus validating the measurement method. Two density inversion points were recorded for this system. We found that the lower density inversion point is not at the minimum temperature of the liquidus curve. This suggests that N_2/CH_4 may not be a eutectic system. However, our experiments cannot determine whether there are one or two types of solid present at this point. Thus, we cannot confirm whether this system has just an azeotrope or a peritectic followed by an azeotrope. Nevertheless, if combined with the results from x-ray diffraction, which indicates the presence of an invariant point, then a peritectic followed by an azeotrope can be inferred and becomes a strong challenge for the long-predicted eutectic. It is still an open question to be investigated until decisive evidence is obtained.

For the CO/CH_4 binary, there is currently no experimental data at low temperatures in the literature. The resulting SLV curve is similar to that of N_2/CH_4. Two density inversion points were observed. Like N_2/CH_4, the minimum SLV temperature is not at the same point as the lower density inversion, indicating an azeotrope with or without a peritectic. However, again, further investigations are needed to confirm which.

For N_2/CO, our SLV pressure data are also the first measured. While a maximum pressure point is present, there are no density inversion points. For this system, the solid always sinks in its liquid. Finally, for N_2/C_2H_6, new SLV pressure data at higher temperatures near the triple point of C_2H_6 and lower temperatures near the triple point of N_2 were measured. The laboratory setup is not currently able to reach the high pressures where these two groups of data meet at the quadruple point (where four phases are in equilibrium—VLLS). This opens a future extension of the method to high-pressure regions.

As there is a scarcity in SLV databases for binary mixtures at cryogenic temperatures and many of them are decades old, this method may be further developed for more accurate new measurements on mixtures with disputable phase diagrams, such as the aforementioned argon/methane and argon/nitrogen, and implemented on other materials in future studies, e.g., combinations of argon, ethane, nitrogen, ethylene, propane, methane, carbon

dioxide, etc. For the next stage of development, we plan to implement measurement of the *in situ* composition to obtain the liquidus curve simultaneously with the three-phase SLV pressure data.

SUPPLEMENTARY MATERIAL

See the supplementary material for the temperature and pressure data points plotted in the figures of this paper. These data points were obtained in the Astrophysical Materials Laboratory at Northern Arizona University using the described experimental method. The dates each experiment was performed on are also listed in the supplementary material.

ACKNOWLEDGMENTS

This work was supported by NASA Solar System Workings Grant No. 80NSSC19K0556 and by a grant from the John and Maureen Hendricks Charitable Foundation. Members of Lowell Observatory's Slipher Society contributed funds for purchase of the temperature-compensated pressure gauge.

AUTHOR DECLARATIONS

Conflict of Interest

The authors have no conflicts to disclose.

Author Contributions

Shaelyn M. Raposa: Data curation (lead); Methodology (lead); Writing – original draft (equal); Writing – review & editing (lead). **Sugata P. Tan:** Methodology (equal); Writing – original draft (lead); Writing – review & editing (equal). **William M. Grundy:** Writing – original draft (supporting); Writing – review & editing (supporting). **Gerrick E. Lindberg:** Writing – original draft (supporting); Writing – review & editing (supporting). **Jennifer Hanley:** Writing – review & editing (supporting). **Jordan K. Steckloff:** Writing – original draft (supporting); Writing – review & editing (supporting). **Stephen C. Tegler:** Writing – review & editing (supporting). **Anna E. Engle:** Writing – review & editing (supporting). **Cecilia L. Thieberger:** Writing – review & editing (supporting).

DATA AVAILABILITY

The data that support the findings of this study are available from the corresponding author upon reasonable request.

REFERENCES

Adidharma, H. and Radosz, M., "The LJ-solid equation of state extended to thermal properties, chain molecules, and mixtures," Ind. Eng. Chem. Res. **43**, 6890–6897 (2004).

Adidharma, H. and Tan, S. P., "Accurate Monte Carlo simulations on FCC and HCP Lennard-Jones solids at very low temperatures and high reduced densities up to 1.30," J. Chem. Phys. **145**, 014503 (2016).

Adidharma, H., Tan, S. P., and Radosz, M., "Prototype of an LJ solid equation of state applied to argon, krypton and methane," Mol. Phys. **100**, 2559–2569 (2002).

Ahrens, C. J., Grundy, W. M., Mandt, K. E., Cooper, P. D., Umurhan, O. M., and Chevrier, V. F., "Recent advancements and motivations of simulated Pluto experiments," Space Sci. Rev. **214**, 130 (2018).

Barreiros, S. F., Calado, J. C. G., Nunes da Ponte, M., and Streett, W. B., "The equation of state and thermodynamic properties of liquid carbon monoxide," J. Chem. Thermodyn. **14**, 1197 (1982).

Barrett, C. S. and Meyer, L., "Argon-nitrogen phase diagram," J. Chem. Phys. **42**, 107–112 (1965).

Browning, C. W., "Phase boundary determinations of binary mixtures at low temperatures," Adv. Cryog. Eng. **9**, 177–187 (1964).

Brown, G. N. and Ziegler, W. T., "Vapor pressure and heats of vaporization and sublimation of liquids and solids of interest in cryogenics below 1-atm pressure," Adv. Cryog. Eng. **25**, 662 (1979).

Bücker, D. and Wagner, W., "A reference equation of state for the thermodynamic properties of ethane for temperatures from the melting line to 675 K and pressures up to 900 MPa," J. Phys. Chem. Ref. Data **35**, 205–266 (2006).

Campestrini, M., Stringari, P., and Arpentinier, P., "Solid–liquid equilibrium prediction for binary mixtures of Ar, O_2, N_2, Kr, Xe, and CH_4 using the LJ-SLV-EoS," Fluid Phase Equilib. **379**, 139–147 (2014).

Clayton, J. O. and Giauque, W. F., "The heat capacity and entropy of carbon monoxide. Heat of vaporization. Vapor pressures of solid and liquid. Free energy to 5000 K. From spectroscopic data," J. Am. Chem. Soc. **54**(7), 2610–2626 (1932).

Clusius, K., Endtinger, F., and Schleich, K., "Results of low-temperature research XXX. The vapour pressure difference of $^{12}CH_4$ and $^{13}CH_4$ between the melting and boiling points," Helv. Chim. Acta **43**(5), 1267–1274 (1960).

Din, F., *Thermodynamic Functions of Gases* (Butterworths, London, 1962), Vol. I.

Eike, D. M. and Maginn, E. J., "Atomistic simulation of solid-liquid coexistence for molecular systems: Application to triazole and benzene," J. Chem. Phys. **124**, 164503 (2006).

Engle, A. E., Hanley, J., Dustrud, S., Thompson, G., Lindberg, G. E., Grundy, W. M., and Tegler, S. C., "Phase diagram for the methane–ethane system and its implications for Titan's lakes," Planet. Sci. J. **2**, 118 (2021).

Espinosa, J. R., Sanz, E., Valeriani, C., and Vega, C., "On fluid-solid direct coexistence simulations: The pseudo-hard sphere model," J. Chem. Phys. **139**, 144502 (2013).

Fastovsky, V. G. and Krestinskii, Y. A., "Solubility of solid methane in liquid nitrogen and oxygen," Zh. Fiz. Khim. **15**, 525–531 (1941).

Federova, M., "Binary mixtures of substances melting at low temperatures," Zh. Eksp. Teor. Fiz. **8**, 425 (1938).

Fray, N. and Schmitt, B., "Sublimation of ices of astrophysical interest: A bibliographic review," Planet. Space Sci. **57**, 2053 (2009).

Fukushima, E., Gibson, A. A. V., and Scott, T. A., "Pressure dependence of the melting and α-β phase transition temperatures of carbon monoxide," J. Low Temp. Phys. **28**, 157–165 (1977).

Goodwin, R. D., "Carbon monoxide thermophysical properties from 68 to 1000 K at pressures to 100 MPa," J. Phys. Chem. Ref. Data **14**, 849–932 (1985).

Gross, J. and Sadowski, G., "Perturbed-chain SAFT: An equation of state based on a perturbation theory for chain molecules," Ind. Eng. Chem. Res. **40**, 1244–1260 (2001).

Grundy, W. M., Morrison, S. J., Bovyn, M. J., Tegler, S. C., and Cornelison, D. M., "Remote sensing D/H ratios in methane ice: Temperature-dependent absorption coefficients of CH_3D in methane ice and in nitrogen ice," Icarus **212**(2), 941–949 (2011).

Hartwig, J., Meyerhofer, P., Lorenz, R., and Lemmon, E., "An analytical solubility model for nitrogen–methane–ethane ternary mixtures," Icarus **299**, 175–186 (2018).

Hofgartner, J. D. and Lunine, J. I., "Does ice float in Titan's lakes and seas?," Icarus **223**, 628–631 (2013).

Kim, J. and Straub, J. E., "Generalized simulated tempering for exploring strong phase transitions," J. Chem. Phys. **133**, 154101 (2010).

Llave, F. M., Luks, K. D., and Kohn, J. P., "Three-phase liquid-liquid-vapor equilibria in the binary systems nitrogen + ethane and nitrogen + propane," J. Chem. Eng. Data **30**, 435–438 (1985).

Long, H. M. and Di Paolo, F. S., "Condensed phase diagram of the system argon-nitrogen," Chem. Eng. Prog. Symp. Ser. **59**(44), 30–35 (1963).

Malaska, M. J., Hodyss, R., Lunine, J. I., Hayes, A. G., Hofgartner, J. D., Hollyday, G., and Lorenz, R. D., "Laboratory measurements of nitrogen dissolution in Titan lake fluids," Icarus **289**, 94–105 (2017).

Matsumoto, M., Saito, S., and Ohmine, I., "Molecular dynamics simulation of the ice nucleation and growth process leading to water freezing," Nature **416**, 409–413 (2002).

Maytal, B. Z. and Pfotenhauer, J. M., *Miniature Joule–Thomson Cryocooling: Principles and Practice* (Springer Science & Business Media, 2012).

McKinnon, W. B., Nimmo, F., Wong, T., Schenk, P. M., White, O. L., Roberts, J. H., Moore, J. M., Spencer, J. R., Howard, A. D., Umurhan, O. M., Stern, S. A., Weaver, H. A., Olkin, C. B., Young, L. A., and Smith, K. E., "Convection in a volatile nitrogen-ice-rich layer drives Pluto's geological vigour," Nature **534**, 82–85 (2016).

Moore, J. M., Howard, A. D., Umurhan, O. M., White, O. L., Schenk, P. M., Beyer, R. A., McKinnon, W. B., Spencer, J. R., Grundy, W. M., Lauer, T. R., Nimmo, F., Young, L. A., Stern, S. A., Weaver, H. A., Olkin, C. B., and Ennico, K., "Sublimation as a landform-shaping process on Pluto," Icarus **287**, 320–333 (2017).

Moores, J. E., Smith, C. L., Toigo, A. D., and Guzewich, S. D., "Penitentes as the origin of the bladed terrain of Tartarus Dorsa on Pluto," Nature **541**, 188–190 (2017).

Moran, D. W., "Low temperature equilibria in binary systems, including the solid phases," Ph.D. thesis, University of London, 1959.

Muniz, M. C., Gartner, T. E, III, Riera, M., Knight, C., Yue, S., Paesani, F., and Panagiotopoulos, A. Z., "Vapor–liquid equilibrium of water with the MB-pol many-body potential," J. Chem. Phys. **154**, 211103 (2021).

Omar, M. H., Dokoupil, Z., and Schroten, M. H. G. M., "Determination of the solid-liquid equilibrium diagram for the nitrogen-methane system," Physica **28**, 309–329 (1962).

Pinnick, E. R., Erramilli, S., and Wang, F., "Predicting the melting temperature of ice-Ih with only electronic structure information as input," J. Chem. Phys. **137**, 014510 (2012).

Porras Giraldo, A. F., Rodriguez-Reartes, S. B., and Zabaloy, M. S., "A solid solution modeling approach somehow analogous to the EoS approach for fluids: Application to equilibria involving fluid phases and solid solutions," Fluid Phase Equilib. **547**, 113174 (2021).

Prokhvatilov, A. I. and Yantsevich, L. D., "X-ray investigation of the equilibrium phase diagram of CH_4-N_2 solid mixtures," Sov. J. Low Temp. Phys. **9**, 94–98 (1983).

Qiu, X., Tan, S. P., Dejam, M., and Adidharma, H., "Novel isochoric measurement of the onset of vapor–liquid phase transition using differential scanning calorimetry," Phys. Chem. Chem. Phys. **20**, 26241–26248 (2018).

Ricci, J. E., *The Phase Rule and Heterogeneous Equilibrium* (D. Van Nostrand Company, Inc., New York, 1951).

Robinson, L. B., "Phase equilibria in cryogenic mixtures: Part II," Cryocoolers **8**, 559–567 (1995).

Roe, H. G. and Grundy, W. M., "Buoyancy of ice in the CH_4–N_2 system," Icarus **219**, 733–736 (2012).

Ruhemann, M., Lichter, A., and Komarov, P., "Zustandsdiagramme niedrig schmelzender gemische: 2 Das schmelzdiagramm sauerstoff-stickstoff und das zustandsdiagramm stickstoff-kohlenoxyd," Phys. Z. Sowjetunion **8**, 326 (1935).

Scott, T. A., "Solid and liquid nitrogen," Phys. Rep. **27**, 89–157 (1976).

Shinoda, T., "Vapor pressure of carbon monoxide in condensed phases," Bull. Chem. Soc. Jpn. **42**, 2815 (1969).

Span, R., Lemmon, E. W., Jacobsen, R. T., Wagner, W., and Yokozeki, A., "A reference equation of state for the thermodynamic properties of nitrogen for temperatures from 63.151 to 1000 K and pressures to 2200 MPa," Phys. Chem. Ref. Data **29**, 1361 (2000).

Steckloff, J. K., Soderblom, J. M., Farnsworth, K. K., Chevrier, V. F., Hanley, J., Soto, A., Groven, J. J., Grundy, W. M., Pearce, L. A., Tegler, S. C., and Engle, A., "Stratification dynamics of Titan's lakes via methane evaporation," Planet. Sci. J. **1**, 26 (2020).

Tan, S. P. and Kargel, J. S., "Multiphase-equilibria analysis: Application in modeling the atmospheric and lacustrine chemical systems of Saturn's moon Titan," Fluid Phase Equilib. **458**, 153–169 (2018a).

Tan, S. P. and Kargel, J. S., "Solid-phase equilibria on Pluto's surface," Mon. Not. R. Astron. Soc. **474**, 4254–4263 (2018b).

Tan, S. P., Kargel, J. S., and Marion, G. M., "Titan's atmosphere and surface liquid: New calculation using Statistical Associating Fluid Theory," Icarus **222**(1), 53–72 (2013).

Tegler, S. C., Grundy, W. M., Olkin, C. B., Young, L. A., Romanishin, W., Cornelison, D. M., and Khodadadkouchaki, R., "Ice mineralogy across and into the surfaces of Pluto, Triton, and Eris," Astrophys. J. **751**, 76 (2012).

Tegler, S. C., Stufflebeam, T. D., Grundy, W. M., Hanley, J., Dustrud, S., Lindberg, G. E., Engle, A., Dillingham, T. R., Matthew, D., Trilling, D., Roe, H., Llama, J., Mace, G., and Quirico, E., "A new two-molecule combination band as a diagnostic of carbon monoxide diluted in nitrogen ice on Triton," Astron. J. **158**, 17 (2019).

Teller, M. and Knapp, H., in *Solid-Liquid Equilibrium Data Collection: Binary Systems*, Chemistry Data Series Vol. VIII, edited by Knapp, H., Teller, M., and Langhorst, R. (Dechema, Frankfurt, 1984; 1987), Part I, p. 32.

Trafton, L. M., Matson, D. L., and Stansberry, J. A., "Surface/atmosphere interactions and volatile transport (Triton, Pluto, and Io)," in *Solar System Ices* (Springer, Dordrecht, 1998), pp. 773–812.

Trowbridge, A. J., Melosh, H. J., Steckloff, J. K., and Freed, A. M., "Vigorous convection as the explanation for Pluto's polygonal terrain," Nature **534**, 79–81 (2016).

Van 'T Zelfde, P., Omar, M. H., Le Pair-Schroten, M. H. G. M., and Dokoupil, Z., "Solid-liquid equilibrium diagram for the argon-methane system," Physica **38**, 241–252 (1968).

Veith, H. and Schröder, E., "Schmelzdiagramme einiger binärer systeme aus kondensierten gasen," Z. Phys. Chem. **179A**, 16–22 (1937).

Verschoyle, T. T. H., "The ternary system carbon monoxide-nitrogen-hydrogen and the component binary systems between temperatures of −185° and −215 °C, and between pressures of 0 and 225 atm," Philos. Trans. R. Soc. London, Ser. A **230**, 189 (1931).

Vetter, M., Jodl, H.-J., and Brodyanski, A., "From optical spectra to phase diagrams—The binary mixture N_2–CO," Low Temp. Phys. **33**, 1052–1060 (2007).

Wales, D. J., "Decoding the energy landscape: Extracting structure, dynamics and thermodynamics," Philos. Trans. R. Soc., A **370**, 2877–2899 (2012).

Wisotzki, K. D. and Schneider, G. M., "Fluid phase equilibria of the binary systems N_2 + ethane and N_2 + pentane between 88 K and 313 K and at pressures up to 200 MPa," Ber. Bunsengesellschaft Phys. Chem. **89**, 21–25 (1985).

Yokozeki, A., "Analytical equation of state for solid-liquid-vapor phases," Int. J. Termophys. **24**, 589–620 (2003).

Younglove, B. A. and Ely, J. F., "Thermophysical properties of fluids. II. Methane, ethane, propane, isobutane, and normal butane," Phys. Chem. Ref. Data **16**, 577–798 (1987).

Zhuang, L., Wang, R., Lindberg, G. E., Hu, H., Li, X.-Z., and Wang, F., "From a liquid to a crystal without going through a first-order phase transition: Determining the free energy of melting with glassy intermediates," J. Phys. Chem. B **123**, 7740–7747 (2019).